RSC Advances

PAPER

View Article Online
View Journal | View Issue

Check for updates

Cite this: *RSC Adv.*, 2025, **15**, 13561

Development of advanced drug-loaded graphene quantum dots with improved photoluminescence properties for enhanced targeted therapy and nano-imaging technologies

Kenza Elkabiri, [ab] Hala Ouarrad [ab] and Lalla Btissam Drissi *[abc]

In this study, a new system of drug-functionalized graphene quantum dots (GQDs) is presented for combined therapeutic delivery and imaging. To do this, doxorubicin (DOX), which is a strong anticancer reagent, is chosen due to its organic nature. Additionally, to investigate quantum confinement effects on the system's efficiency, diamond-shaped GQDs with two different sizes are utilized. We theoretically investigate the optoelectronic and photoluminescence behavior of various drug-GQD arrangements, to evaluate their nanomedical diagnostic efficiency. The findings confirm the accuracy of the systems investigated. The stability of the hybrid structures is confirmed by the absence of imaginary frequencies. As the size of GQD increases, the HOMO–LUMO gap energy decreases under the regulation of drug binding and nanoparticles hardness. This size-dependent effect also causes a red-shift in the optical emission and absorption spectra upon DOX conjugation. Furthermore, DOX-conjugated GQDs exhibit strong near-infrared photoluminescence, suggesting their application potential in drug delivery and diagnostics in nanomedicine.

Received 10th November 2024
Accepted 24th March 2025

DOI: 10.1039/d4ra07998a

rsc.li/rsc-advances

Open Access Article. Published on 28 April 2025. Downloaded on 1/19/2026 3:58:13 AM.
This article is licensed under a Creative Commons Attribution-NonCommercial 3.0 Unported Licence.

1. Introduction

Graphene discovery has stimulated wide studies and interest across numerous scientific and engineering disciplines[1] owing to its excellent properties,[2,3] such as high electrical conductivity,[4,5] broad optical absorption and emission,[6] chemical stability, and biocompatibility, leading to a wide range of applications in biomedicine and electronics. These applications include cancer diagnostics and treatment through drug delivery, bioimaging and tissue engineering,[7,8] in addition to electronic novel technologies such as high-speed transistors, flexible circuits, sensors, and photodetectors.[9] Consequently, extensive efforts have been made to develop methods for producing and manipulating graphene and its derivatives, including graphene quantum dots.[10]

Despite the numerous advantages of pristine graphene, its applications are limited by several challenges. One major issue is its zero band gap,[11] which adversely affects its absorption properties.[12] In order to overcome these limitations, various approaches have been explored, including chemical modifications utilizing functional groups, the development of new graphene-based 2D nanostructured composites through atomic combinations and hyridization,[13] and the introduction of quantum confinement effects by forming nanoribbons or quantum dots.[14–16]

Among the better alternatives of graphene 2D sheets, are graphene quantum dots (GQDs). GQDs – as small fragments of graphene with a diameter of <20 nm[17] – have drawn sufficient attention due to their unique characteristics. Such nanomaterials can be synthesized in varied geometries, *i.e.*, hexagonal, triangular, diamond, and rectangular.[18–21] Originally synthesized in 2008,[22] GQDs differ from bulk graphene through the occurrence of a band gap owing to quantum confinement effects and alterations in their surface properties.[23] They also exhibit tunable photoluminescence, excellent photostability, and low toxicity, making them perfect for a wide range of optoelectronic and nanomedical applications such as solar cells,[24,25] bio-imaging, sensing, light-emitting diodes, and display technologies.[26–30]

Remarkably, the electronic, optical, and excitonic properties of GQDs can be controlled through morphological modification like size, shape and edge termination tuning,[31,32] or through chemical modification like surface and edge functionalization.[33] The energy gap of GQDs is notably affected by their size and shape, with the larger GQDs presenting a reduced gap, particularly those consisting of specific numbers of conjugated carbon atoms. This trend has been confirmed both theoretically by calculations using density functional theory (DFT)[34] and

[a]*LPHE, Modeling & Simulations, Faculty of Science, Mohammed V University in Rabat, Rabat, Morocco. E-mail: ldrissi@fsr.ac.ma*

[b]*CPM, Centre of Physics and Mathematics, Faculty of Science, Mohammed V University in Rabat, Rabat, Morocco*

[c]*College of Physical and Chemical Sciences, Hassan II Academy of Sciences and Technology, Rabat, Morocco. E-mail: b.drissi@academiesciences.ma*

© 2025 The Author(s). Published by the Royal Society of Chemistry

Open Access Article. Published on 28 April 2025. Downloaded on 1/19/2026 3:58:13 AM. This article is licensed under a Creative Commons Attribution-NonCommercial 3.0 Unported Licence.

experimentally in GQD samples obtained by hydrothermal cutting of graphene sheets.[35] Besides, GQDs with zigzag edges are shown to possess more favorable electronic properties as the zigzag edge pattern significantly influences the nature of frontier molecular orbitals (FMO), *i.e.*, the highest occupied molecular orbital (HOMO) and lowest unoccupied molecular orbital (LUMO).[36] While on the other hand, the chemical modification using functionalization, helps to tune the optoelectronic properties of GQDs, as was revealed through theoretical studies of Janus pyrene and coronene.[37] Furthermore, experimentally it has been shown that heteroatom doping of GQDs using atoms like boron, nitrogen, sulphur and oxygen, heavily enhances their electronic, optical, and photoluminescence.[38–41]

Beyond functionalizing GQDs with various heteroatoms and chemical groups, another method involves conjugation with large molecules such as photosensitizers or biomolecules.[42,43] This conjugation can be done through different types of interactions such as hydrogen binding, covalent binding, and van der Waals interactions (such as π–π stacking).[44]

One of the most critical properties that make GQDs highly effective as drug carriers is their exceptionally large surface area, which allows for high drug-loading capacity and efficient molecular interactions.[45] This characteristic enhances the capacity of GQDs to carry therapeutic agents, making them effective nanocarriers in drug delivery applications. Additionally, unlike some other quantum dots or graphene oxide sheets, GQDs are considered to be less toxic and more biocompatible,[46] which is crucial for biomedical applications, including drug delivery.

In this regard, extensive efforts have been focused on the functionalization of GQD nanoparticles with organic molecules for therapeutic use, including *in vivo* and *in vitro* bioimaging and targeted drug delivery for cancer treatment.[47] GQDs have also been explored as drug nanocarriers for drugs like doxorubicin (DOX), exhibiting great biocompatibility and targeted drug release. Their multimodal conjugation feature also makes it possible to incorporate ligands to minimize side effects.[48,49] Likewise, methotrexate was effectively loaded into nitrogen-doped GQDs through effective π–π stacking interactions and was used to treat breast cancer cells *in vivo*.[50] Another work has focused on loading the anticancer drug doxorubicin (DOX) onto GQDs by van der Waals interactions, triggered by pH-responsive release and photothermal effects *in vitro*.[51] Likewise, a hydrogen-bonded cross-linked CMC–GQD–DOX system was also pH-sensitive.[52] In yet another approach, water-dispersible GQDs were derived from pristine multi-walled carbon nanotubes (MWCNT) and covalently attached to an anticancer drug.[53] Such GQD–DDS was highly cytocompatible and enhanced the interaction between drugs and cells.

Building on previous research, this study aims to conduct an in-depth analysis of the behaviour of GQDs under structural modifications, particularly functionalization with an organic molecule, to develop a robust drug delivery system. Most prior studies in this field have focused on non-covalent interactions, such as van der Waals or hydrogen bonds, for structuring drug delivery systems. However, covalent bonds are known to be stronger and more stable under varying environmental conditions, such as changes in pH. Given these advantages, we aim to investigate the potential of covalently bonded systems for enhanced drug delivery applications and explore the possibility of developing a more resilient system. Additionally, this study seeks to gain a deeper understanding of the properties of GQDs and their behaviour, in response to different functionalization strategies. Specifically, we examine factors influencing the band gap and photoluminescence of GQDs, including coupling effects with the anticancer drug DOX and the impact of hybridization across different GQD sizes. To achieve this, we analyse the coupling of two different sizes of GQDs with DOX, a widely used drug in drug carriers and other delivery systems. Using density functional theory (DFT), three systems are designed for each GQD size, incorporating the distinct covalent interactions C–O, C– C, and C–N couplings. The resulting electronic and optical properties are then evaluated to determine the most favourable interactions for optimizing drug delivery performance. The main scope of this study is investigating the covalent coupling of two different sized GQDs with DOX, focusing on specific carbon-based interactions at the zigzag edges of the GQDs. Regarding DOX ($C_{27}H_{29}NO_{11}$), it is a common chemotherapy agent used to treat many types of cancers, such as lung and breast cancer, and is overall safe to use.[48,49] It can, however, lead to organ damage, especially to the heart, in certain instances. This side effect can be reduced by co-administration with vitamin E.[54] Interestingly, unlike previous studies that have explored DOX–GQD interactions,[55] our research extends these investigations by systematically examining the influence of the various interaction types – C–C, C–N, and C–O – on the electronic properties and stability of the drug–GQD system. In addition, by considering both small and large-sized GQDs, we provide a detailed analysis of how the size and interaction type affect the electronic properties, such as the HOMO–LUMO gap and chemical hardness. Our findings indicate that systems featuring C–O interactions exhibit the highest band gap, absorption, and emission energies. Additionally, all GQD + DOX hybrid systems demonstrate emission wavelengths in the near-infrared region, with larger GQDs exhibiting more pronounced photoluminescence. These insights contribute to the development of an optimized drug delivery platform based on covalently functionalized GQDs.

This paper is organized as follows: the first section presents the computational methodology employed. The second section presents the principal results and discussion. The third and last section gives a conclusion of the main points.

2. Computational methods

All calculations were conducted within the framework of density functional theory (DFT) at B3LYP exchange–correlation functional and 6-31G(d,p) basis set,[56,57] using the Gaussian 09 software package. B3LYP, or the three-parameter hybrid Becke plus the Lee–Yang–Parr correlation functional, is known to be accurate as well as applicable for electronic property computations of big molecules.[58] Its success lies in the fact that it is a mixture of a fraction of exact exchange *via* the adiabatic

© 2025 The Author(s). Published by the Royal Society of Chemistry

Open Access Article. Published on 28 April 2025. Downloaded on 1/19/2026 3:58:13 AM. This article is licensed under a Creative Commons Attribution-NonCommercial 3.0 Unported Licence.

connection formula, differentiating it from other methods of DFT.[59] Additionally, the choice of B3LYP/6-31G(d) is supported by its proven precision in computational chemistry, as demonstrated in previous studies.[60,61] This functional is widely recognized as one of the most reliable methods for studying quantum dots, even for large systems. Moreover, B3LYP has been successfully applied in modelling large drug delivery systems, including doxorubicin-based systems.[62] The 6-31G(d) basis set is particularly well-suited for nanostructures due to its balance between computational cost and accuracy, making it a practical choice for investigating the optoelectronic properties of GQD–DOX systems. Specifically, B3LYP combines Hartree–Fock (HF) exchange with the Vosko, Wilk, and Nusair[63] functional III for local correlation and the Lee–Yang–Parr (LYP) correlation functional for non-local correlation. The B3LYP exchange–correlation energy ($E_{xc}^{B3LYP}[\rho]$) is expressed as follows:[64]

$$E_{xc}^{B3LYP}[\rho] = E_{xc}^{SVWN} + c_1(E_x^{exact} - E_x^S) + c_2\Delta E_X^B + c_3\Delta E_C^{LYP} \quad (1)$$

In this equation, E_{xc}^{SVWN} represents the exchange–correlation energy using the Slater–Vosko–Wilk–Nusair (SVWN) exchange–correlation functional, while E_x^{exact} denotes the exact exchange–correlation. The terms ΔE_X^B and ΔE_C^{LYP} correspond to the gradient-containing correction terms to the LDA exchange–correlation. The constants $c_1 = 0.20$, $c_2 = 0.72$, and $c_3 = 0.81$, are empirically derived from fitting to experimental thermochemical data from the G2 set.

The investigated systems were optimized in their ground state. The stability of our systems, specifically the GQD bonded to the molecule, was evaluated by calculating the binding energy using eqn (2):

$$\Delta E = E_T - E_{GQD} - E_{Drug} \quad (2)$$

where E_T presents the optimized total energy of the whole system (GQD + drug), and E_{GQD} and E_{Drug} are the optimized energies of the GQD and the drug molecule, respectively.

The HOMO–LUMO (H–L) energy gap presented in this work was determined using eqn (3):

$$E_g = E^{LUMO} - E^{HOMO}. \quad (3)$$

Furthermore, the global reactivity indices including chemical potential (μ) and chemical hardness (η) are calculated using the following equations:[65]

$$\mu = -\chi = \frac{IP + EA}{2}, \text{ and } \eta = \frac{IP - EA}{2} \quad (4)$$

where the ionization potential (IP) is defined as $IP = -E^{HOMO}$, while the electron affinity (EA) is given by $EA = -E^{LUMO}$. Notice that the electrophilicity (ω) is defined as follows:

$$\omega = \frac{\mu^2}{\eta}. \quad (5)$$

Finally, the UV-Vis calculations were performed using the time-dependent self-consistent field (TD-SCF) calculations to study the excited states. All the UV-Vis calculations were performed by selecting $n = 20$ states for higher accuracy.

3. Results and discussion

In this section, we explore the influence of functionalizing diamond-shaped graphene quantum dots (DSGQDs) with the organic molecule $C_{27}H_{29}NO_{11}$ (the DOX drug) *via* three different types of coupling interactions. We start by analysing the properties of two various sizes of pristine DSGQDs and the target molecule. Then, we observe how their properties are modified upon functionalization depending on the nature of interaction. Careful comparisons of the results obtained are therefore presented, aiming to identify the most effective functionalization pathway for DSGQDs and with potential application in the area of nanomedicine.

3.1. Pristine GQDs and the DOX drug molecule

3.1.1. Structural details. This study investigates two different sizes of DSGQDs, *i.e.*, $C_{30}H_{14}$ and $C_{48}H_{18}$, as shown in Fig. 1(a) and (b). The smaller GQD comprise 30 carbon and 14 hydrogen atoms, while the larger one has 48 carbon and 18 hydrogen atoms. Both GQDs are made of a mixture of zigzag edges and armchair corners with complete hydrogen-passivated dangling bonds, to guarantee more energetic stability. The bond angles and C–C bond lengths are approximately 1.4 Å and 120°, respectively, in good agreement with previous research on smaller C, Si, and CSi hybrid diamond-shaped quantum dots.[31] The average sizes of the GQDs are approximately 1.233 nm for the GQD-30 and 1.665 nm for the GQD-48, aligning well with data from ref. 20. These two sizes were chosen to investigate the interplay between quantum confinement effects and functionalization mechanism which depends on the different couplings between GQD and DOX. Besides, we focus on key factors that significantly influence the toxicity of our DSGQDs, including their small size, specific shape, and the presence of organic functional groups. These characteristics are intended to minimize *in vitro* and *in vivo* toxicity. Small-sized GQDs exhibit negligible toxicity compared to graphene oxide-based nanoparticles.[66]

Our main aim is to find the optimum configuration for the transportation of the drug molecule $C_{27}H_{29}NO_{11}$, shown in Fig. 1(c), in order to maximize performance in medical applications. As the focus has been put on biomedical uses and safety, determination of the toxicity of the GQDs is essential. Toxicity in graphene-based nanomaterials is altered by factors such as size, shape, surface functional groups, type of ligand, surface charges, and interaction with other molecules under biological conditions.[30,47] Additional factors such as bioactivity of exterior layers and mechanical stability could also impact toxicity.[28] This work emphasizes the behaviour of small size and shape GQDs conjugated to organic functional groups, namely DOX, in order to minimize *in vitro* and *in vivo* toxicity. This has been substantiated by previous reports showing that small-sized GQDs are less toxic compared to graphene oxide-based nanoparticles.[66]

Open Access Article. Published on 28 April 2025. Downloaded on 1/19/2026 3:58:13 AM.
This article is licensed under a Creative Commons Attribution-NonCommercial 3.0 Unported Licence.

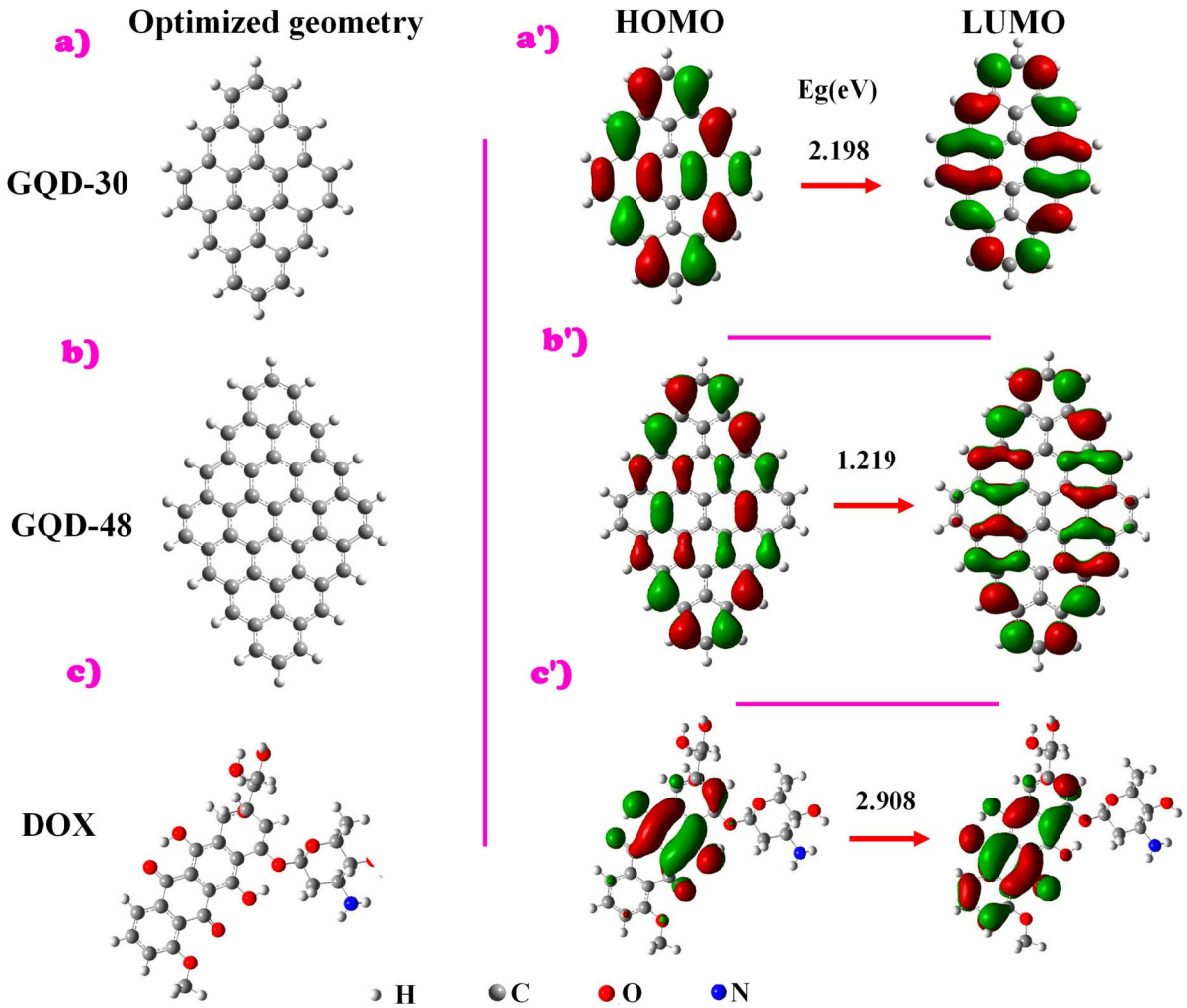

Fig. 1 (Left) Optimised molecular structures of the DSGQDs (a) $C_{30}H_{14}$ and (b) $C_{48}H_{18}$, as well as (c) $C_{27}H_{29}NO_{11}$. (Right) (a′–c′) Frontier molecular orbital plots of $C_{30}H_{14}$, $C_{48}H_{18}$ and $C_{27}H_{29}NO_{11}$.

3.1.2. Electronic properties. The electronic properties of the pristine systems are investigated by analysing their energy gap behaviour, with the corresponding values detailed in Table 1. This analysis provides valuable insights into the electronic structure and stability of the systems. E_g values computed for both GQD-30 and GQD-48 are 2.198 eV and 1.219 eV, respectively. Interestingly, a significant reduction was noticed in the H–L gap with the increase in GQD size, which is consistent with previous studies.[31,35,67] The underlying reason behind this finding is that smaller GQDs possess pronounced quantum confinement. The same observation can be made regarding graphene and silicene QDs in nanomedical diagnostics, for which the DFT-GGA and GW calculations were performed to explore their electronic properties.[33]

Concerning the DOX molecule $C_{27}H_{29}NO_{11}$, the H–L energy value is 2.908 eV which is a larger energy gap than both DSGQDs (see Table 1). This result is mainly attributed to the small size of DOX molecule as compared to the studied QDs (see Fig. 1).

To gain more insight on the electronic behaviour of pristine systems, the electron charge density was determined and is

Table 1 Calculated values of the HOMO, LUMO and band gap energies E_g, absorption E_{abs} and emission E_{em} energies, absorption λ_{abs} and emission wavelengths λ_{em} of GQDs and DOX using TDDFT. Units are in eV for energies and nm for wavelengths

Structure	HOMO	LUMO	E_g	E_{abs}	λ_{abs}	E_{em}	λ_{em}	Stokes shift
$C_{30}H_{14}$	−4.584	−2.386	2.198	2.345	528.72	2.1984	590.75	0.147
$C_{48}H_{18}$	−4.157	−2.937	1.219	1.446	857.299	1.289	954.639	0.157
$C_{27}H_{29}NO_{11}$	−5.375	−2.466	2.908	2.518	492.38	1.727	717.838	0.791

© 2025 The Author(s). Published by the Royal Society of Chemistry

Open Access Article. Published on 28 April 2025. Downloaded on 1/19/2026 3:58:13 AM.
This article is licensed under a Creative Commons Attribution-NonCommercial 3.0 Unported Licence.

plotted in Fig. 1. Notably, the larger GQD-48 possesses greater hybridization of FMO in HOMO and LUMO states compared to the smaller GQD-30. This is most likely due to the fact that GQD-48 possesses a larger surface area and greater available atomic orbitals for interaction, allowing more orbital mixing and more complex molecular orbital patterns. Thus, more hybridization reduces the energy gap between HOMO and LUMO because electrons are distributed across a larger number of orbitals, with closely packed energy levels. These results are consistent with our earlier work on the $C_{16}H_{10}$ and $C_{30}H_{14}$ DSGQDs.[24] For DOX, the HOMO is localized mainly on the centre aromatic rings and also on C–O and O–H bonds of the molecule at the molecule's edges, while the LUMO is distributed around the anthraquinone group. Such localization suggests that the most efficient way of functionalizing QDs with DOX would be through π-electron interaction to enable stacking through van der Waals forces.[68] Yet, in the current work, a covalent bonding strategy is employed to conjugate DSGQDs with DOX, focusing on enhanced stability. A more comprehensive analysis of the stability of the conjugated systems will be provided in the following section.

3.1.3. Optical behaviour. In this section, the optical response of the pristine systems was thoroughly examined by analysing the absorption and emission spectra illustrated in Fig. 2. Both GQDs exhibit strong absorption in the visible and near-infrared spectrum, with $C_{30}H_{14}$ being stronger. For the DOX molecule, its absorption spectrum is red-shifted, exactly enabling it to absorb blue light. This optical property is largely attributed to the polar character, high charge delocalization, and high electron acceptance nature of DOX.[69]

We observe the same behaviour in the emission spectra, where longer wavelengths are observed for the $C_{48}H_{18}$ nanostructure compared to the $C_{30}H_{14}$ QD, consistent with the absorption. Notably, the wavelengths of emission are longer than their respective wavelengths of absorption, which further verifies the photoluminescence character of these structures. Interestingly, DOX itself is photoluminescent, in line with experiments.[70] This property of DOX can be a valuable agent in nanomedical research and bioimaging, especially when combined with the properties of GQD.

Both the emission and absorption spectra get shifted more into the near-ultraviolet (NUV) with the increment of the GQDs size – larger QDs emit at longer wavelengths. This behaviour aligns with experimental studies on the photophysical properties of GQDs of approximately 2 nm and 18 nm, prepared *via* a modified method of graphite intercalation compounds.[71] These GQDs show a red-shift in emission peaks as their size increases. The Stokes shift values, presented in Table 1, indicate a clear sensitivity to size variations in GQDs. The larger GQD exhibits a Stokes shift of 0.157 eV (97.34 nm), which is only slightly higher, by 0.01 eV, compared to the smaller GQD, with a Stokes shift of 0.147 eV (62.02 nm). This observation aligns with previous findings.[33] Notably, GQD-48 demonstrates a larger Stokes shift (over 80 nm), which makes it especially suitable for bioimaging applications.[72] In contrast, the DOX molecule shows a significantly larger Stokes shift of 0.791 eV (225.458 nm), a feature that may influence its coupling behaviour.

Additional discussion is provided through analysing the optical parameters determined by time-dependent density functional theory (TDDFT) calculations. The detailed optical findings are presented in Table 1. Obviously, smaller GQD exhibits a greater capacity to absorb light than the larger one with the absorption value being 2.345 eV for $C_{30}H_{14}$ and 1.446 eV for $C_{48}H_{18}$, QDs. This finding is in full accordance with our previous studies on the size dependence of optoelectronic properties in carbon, silicon, and CSi hybrid diamond QDs.[31,33] A similar behaviour has been found in previous studies that examined the optoelectronic properties of GQDs as a function of size, employing large-scale electron-correlated calculations.[20,73] All of these results reinforce the conclusion that the energy gap is a crucial factor in determining the optical properties of materials. Specifically, systems with smaller band gaps are capable of absorbing lower-energy photons, while those with larger band gaps require higher-energy photons to enable electron transitions between different states. Thus, the obtained results demonstrate that the size of QDs plays a crucial role in controlling their optoelectronic properties. Additionally, the investigation of pristine DOX reveals its promising potential when coupled with DSGQDs. This combination could have

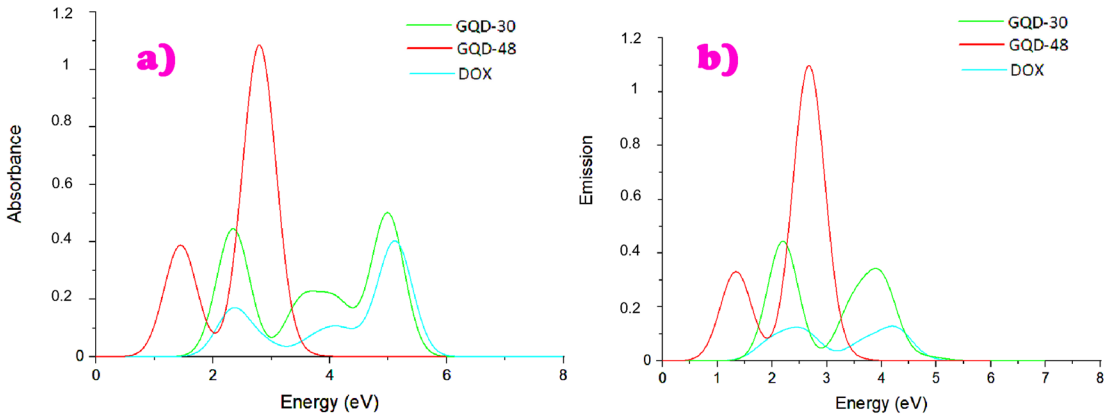

Fig. 2 Absorption and photoluminescence spectra of both GQDs and the DOX molecule, obtained using the TDDFT method.

Open Access Article. Published on 28 April 2025. Downloaded on 1/19/2026 3:58:13 AM.
This article is licensed under a Creative Commons Attribution-NonCommercial 3.0 Unported Licence.

significant implications in the nanomedical field, particularly in applications related to drug delivery and bioimaging, as further discussed below.[74]

3.2. GQDs + drug conjugated systems

The present section investigates the effect of DOX conjugation on the optoelectronic properties and the photoluminescence of the GQDs by analysing the structural properties of the potential new molecules as well as their stability, along with examining their electronic and optical characteristics, and concluding with a discussion and comparison to summarize the major findings.

3.2.1. Structural properties and stability details

3.2.1.1. Structural properties. Building on the findings from the previous section, this study looks at how DOX interacts with the two sizes of GQDs, namely GQD-30 and GQD-48. DOX can connect to GQDs in many ways, influenced by the D_{2h} symmetry of the DSGQDs. There are more than 30 possible ways they can connect under normal conditions. However, since we are focusing on drug delivery, we only look at configurations where a carbon atom from the zigzag edges of the GQDs connects with a carbon, oxygen, or nitrogen atom in the DOX molecule, depicted in Fig. 3 and 4. We choose atoms with the lowest electron density because this helps form weaker covalent bonds. These bonds are strong enough to keep the structure stable but require less energy to break, making it easier to release the drug at the target site. This approach also helps the system withstand different physiological conditions.[75] To make the system even more stable, we avoid hydrogen bonds because

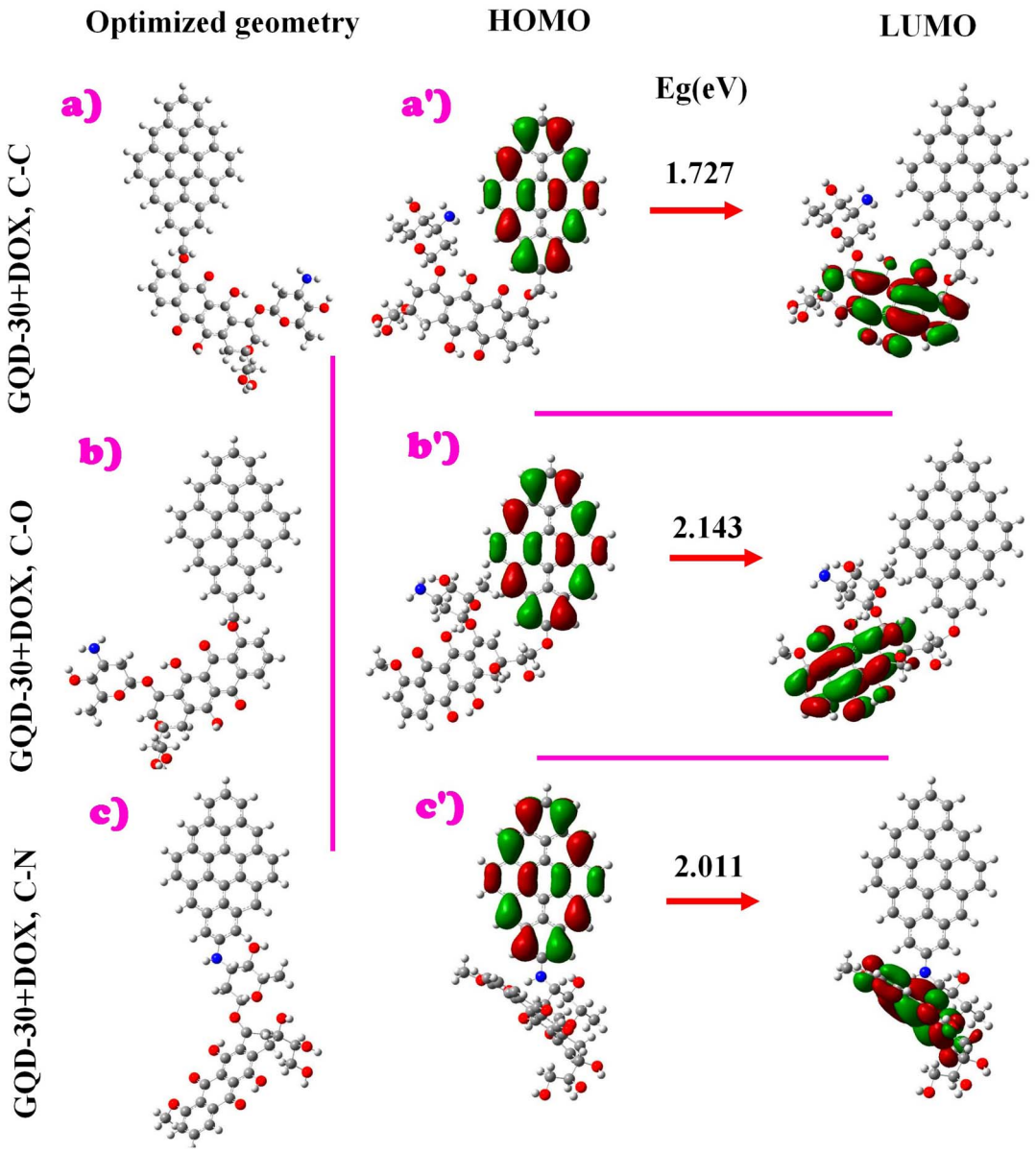

Fig. 3 (a–c) Schematic representation of the molecular structures of the six studied GQD + DOX-30 configurations. Three different systems were generated, featuring different types of bonding: C–C, C–O, and C–N. (a′–c′) The corresponding frontier molecular orbital plots of the studied systems.

© 2025 The Author(s). Published by the Royal Society of Chemistry

Open Access Article. Published on 28 April 2025. Downloaded on 1/19/2026 3:58:13 AM.
This article is licensed under a Creative Commons Attribution-NonCommercial 3.0 Unported Licence.

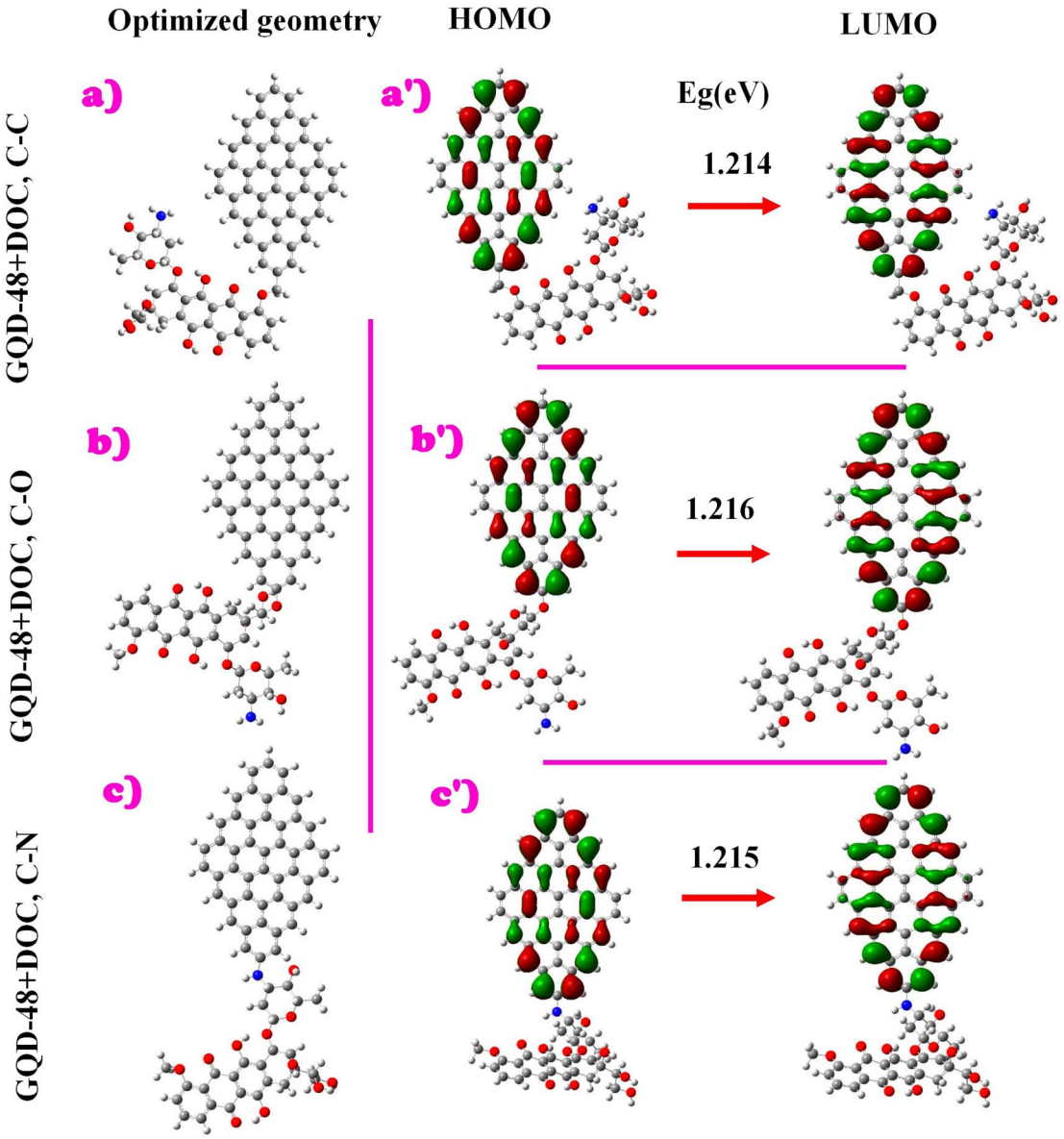

Fig. 4 (a–c) Schematic representation of the molecular structures of the six studied GQD + DOX-48 configurations. Three different systems were generated, featuring different types of bonding: C–C, C–O, and C–N. (a′–c′) The corresponding frontier molecular orbital plots of the studied system.

they are sensitive to pH changes, which could cause the drug to be released too early, as noted in ref. 76.

The DSQDs + DOX structures are categorized into three main groups based on the location of the QD C-atoms on their edges:

(i) Zigzag edge coupling: in the first group, a C atom from the GQD's zigzag edge interacts with a carbon, oxygen, or nitrogen atom on the edge of the DOX molecule. This direct linkage can significantly impact the electronic features, as the FMO of the GQDs are distributed along their zigzag edges, influencing the overall electronic structure of the resulting conjugation.

(ii) Armchair corner coupling: the second category involves a bond between DOX and a C atom at the armchair corner of the DSGQD. This configuration localizes electronic effects, extending the HOMO and LUMO isosurfaces into the armchair corners of the QDs.

(iii) Unpassivated C atom coupling: the third group consists of linkages involving an unpassivated C-atom on the QDs edge. This option may significantly affect electronic properties but is less predictable due to the higher reactivity of the unpassivated carbon atoms.

This study specifically examines six selected structures, as illustrated in Fig. 3 and 4, including three configurations for GQD-30 + DOX and three for GQD-48 + DOX. These structures fall within the first group, where the interaction is achieved by adsorbing one of the DOX atoms (C, O, or N) onto a C atom on the zigzag edge of the QDs. This leads to three distinct types of interaction:

• C–C coupling: structures where a carbon atom from the zigzag edge of the GQD bonds with a carbon atom from DOX.

Open Access Article. Published on 28 April 2025. Downloaded on 1/19/2026 3:58:13 AM. This article is licensed under a Creative Commons Attribution-NonCommercial 3.0 Unported Licence.

• C–N coupling: configurations where a C atom from the GQD binds to the nitrogen atom of $C_{27}H_{29}NO_{11}$.

• C–O coupling: derivatives where the GQD's carbon atom interacts with one of the 11 oxygen atoms present in the DOX molecule.

These targeted configurations are strategically selected to optimize the electronic and optical properties for potential nanomedical applications, particularly in drug delivery and bioimaging.

3.2.1.2. Energetic stability. According to the harmonic frequencies shown in Table 2, the absence of imaginary vibrational modes confirms that all six investigated structures are energetically stable. Even though the three types of interactions (C–C, C–N, and C–O) show similar frequency values due to having the same number of atoms, some structures, particularly those with C–N and C–O interactions, display slightly higher frequencies. This suggests that these bonds contribute more to stability compared to C–C coupling. This observation aligns with previous findings on GQD–anthoxanthin nanocomposites[77] and GQD/phenoxazine-based dyes.[78] In addition to vibrational analysis, the binding energy (E_B), listed in Table 2, also provides insights into structural stability. The results indicate that the $C_{48}H_{18}$ + DOX hybrids are more stable than the smaller $C_{30}H_{14}$ + DOX systems, consistent with earlier studies on drug delivery systems.[79,80] Among all interactions, the C–O coupling shows the highest stability.[81–83]

3.2.1.3. Chemical stability. To better understand the stability of our systems, we calculated the global reactivity indices, including chemical hardness and electrophilicity, as presented in Table 2.

Starting with the chemical hardness that indicates how much a molecule resists changes in its electron distribution. Based on our results, the $C_{30}H_{14}$ QDs with C–C interaction that has the lowest energy gap also has the lowest chemical hardness value ($\eta = 0.863$ eV). In contrast, the system with C–O interaction with the largest energy gap has the highest chemical hardness value (1.072 eV). This suggests that more chemically hard molecules are harder to polarize, cost more energy to excite, and tend to have a large energy gap. Conversely, less chemically hard systems are easier to polarize, more reactive, and tend to donate electrons, which is linked with a smaller HOMO–LUMO energy gap. These are in agreement with previous studies on 4-fluoro-4-hydroxybenzophenone.[84]

Electrophilicity, which measures a molecule's tendency to accept electrons, also varies with the type of interaction. Specifically, it is lowest for the C–O interaction, indicating that the $C_{30}H_{14}$ + DOX system with C–O coupling is the least inclined to accept electrons, thus making it the most stable configuration among the examined structures. This is followed by the C–N interaction, and lastly, the C–C coupling, confirming the trends observed in binding energy and harmonic frequency analyses. This behaviour is linked to chemical potential (μ) and electronegativity, as the more electronegative atom, namely oxygen, followed by nitrogen and then carbon, retains electrons more tightly, enhancing the stability of the corresponding structure. This trend agrees with the theoretical investigations of 4-fluoro-4-hydroxybenzophenone[84] and synthesized diorganotin(IV) 2-chloridophenylacetohydroxamate complexes,[85] where greater stability and chemical hardness are associated with larger energy gaps.

For the $C_{48}H_{18}$ QD systems, all configurations showed similar chemical hardness to the pristine QD, despite different bonding interactions. However, their electrophilicity behaved oppositely to the smaller $C_{30}H_{14}$ + DOX structures, likely due to the consistent hardness across the $C_{48}H_{18}$ + DOX configurations despite increased electronegativity. This suggests that DOX functionalization significantly alters the electronic properties of smaller nanoparticles, while larger systems retain electronic characteristics similar to pure GQDs, highlighting a stronger impact on smaller nanostructures.

3.2.2. Electronic properties. In the present part, we examine the electronic response of GQDs and DOX conjugation by analysing the obtained electronic properties including the H–L energy gap E_g and the electron charge density.

Hybridizing GQDs with DOX affects the electronic properties differently depending on the size of the GQDs. For the smaller GQD-30 systems, the H–L energy gap decreases upon conjugation, with the smallest gap observed for the C–C interaction (1.727 eV), followed by C–N (2.011 eV), and the largest for C–O (2.143 eV). The observed narrowing of the energy gap for GQD-30 + DOX can be attributed to the slight decrease in LUMO energy due to the strong electronic interaction between DOX and GQD-30. This interaction leads to an efficient charge transfer, with DOX acting as an electron acceptor. In contrast, the larger GQD-48 + DOX systems maintain nearly the same energy gap as pristine GQD-48 (1.215–1.216 eV). This stability arises because both HOMO and LUMO levels drop at a similar rate, keeping the energy gap unchanged. This behaviour aligns with observations in other nanocomposites, like GQDs coupled

Table 2 Negative values of HOMO and LUMO energies (E_H and E_L) in eV, frequencies (ν) in cm^{-1}, binding energy in eV, chemical potential (μ), chemical hardness (η), and electrophilicity (ω) values, as well as, HOMO–LUMO energy gap (E_g) of different sizes of GQDs obtained from the ground state in eV of all the structures (GQD + DOX)

	Coupling	−H/−L	ν	E_B	μ	ω	η	E_g
$C_{30}H_{14}$ + DOX	C–C	4.4/2.68	7.1–3769	25.79	−3.542	14.53	0.863	1.727
	C–N	4.6/2.58	4.7–3830	25.82	−3.628	13.08	1.006	2.011
	C–O	4.7/2.56	5.7–3819	23.51	−3.629	12.28	1.072	2.143
$C_{48}H_{18}$ + DOX	C–C	4.0/2.8	5.0–3821	23.03	−3.405	19.1	0.607	1.214
	C–N	4.1/2.9	3.3–3842	25.6	−3.506	20.15	0.61	1.215
	C–O	4.2/3.0	3.1–3838	23.02	−3.603	21.35	0.608	1.216

© 2025 The Author(s). Published by the Royal Society of Chemistry

Open Access Article. Published on 28 April 2025. Downloaded on 1/19/2026 3:58:13 AM. This article is licensed under a Creative Commons Attribution-NonCommercial 3.0 Unported Licence.

with phenoxazine-based dyes for solar cells, where the energy gap of larger configurations remains nearly constant.

Additionally, the proportion of each component in the GQD + DOX nanostructure plays a crucial role. In GQD-48 + DOX systems, the contribution from both GQD and DOX is nearly equal, preserving the electronic characteristics of the pristine GQD. However, in GQD-30 + DOX hybrids, GQD contributes less than 50% to the overall structure, leading to more pronounced changes in electronic properties. This composition-dependent behaviour is consistent with findings from other GQD-based systems, such as magnetic nanoparticles and phenoxazine-dye composites, where the drug loading capacity influences the final properties of the hybrid.

To better understand the observed electronic behaviour, we analyse the electron charge density distribution which provides further explanation. In GQD-48 + DOX systems, no significant charge transfer is observed, and both HOMO and LUMO are mainly localized on the GQD, maintaining electronic properties similar to pristine GQD-48. Conversely, for GQD-30 + DOX systems, HOMO is localized on the GQD, while LUMO is primarily on the DOX molecule, suggesting DOX acts as an electron acceptor due to its lower hybridization LUMO energy. This difference in electronic behaviour is attributed to the size-dependent interaction between GQDs and DOX.

3.2.3. Optical response. The present section explores the optical properties of the GQDs + DOX systems, focusing on their absorption and emission energies as well as the associated spectra, as shown in Table 3 and Fig. 5.

Upon conjugation with the drug molecule, smaller GQD-30 leads to a significant reduction in both absorption and emission energies. In contrast to this, the GQD-48 + DOX systems lead to minor changes. This change is attributed to the size, *i.e.* quantum confinement and relative contribution of individual GQDs in the hybrid structure, as was evidenced by the electron charge density provided in Fig. 3 and 4.

Moreover, the results show that smaller GQDs with weaker covalent bonds lead to greater stability under physiological conditions, enabling controlled drug release at the targeted site, and thus minimizing premature release due to factors such as pH changes.[11] This increased stability is critical for ensuring that the drug remains intact until it reaches its target, thereby enhancing therapeutic efficacy and reducing side effects. Furthermore, the decreased H–L gap for smaller GQDs, combined with more stable binding energies, suggests these systems hold significant potential for improving targeted drug delivery. Additionally, we observe that the C–O interaction leads to the most stable configuration, while the smaller GQD-30 with a C–C interaction shows the lowest energy gap, suggesting more reactivity.

Further analysis of the coupling effect reveals that configurations of C–C interactions always produce the lowest values of absorption and emission, while C–O and C–N interactions produce higher values. These distinctions follow the band gap behaviour as described above: a lower HOMO–LUMO gap is correlated with lower frequencies and longer wavelengths. Interestingly, despite all GQD-48 + DOX configurations sharing identical band gap values, their optical responses vary with the bonding type. For example, GQD-48 + DOX with C–N bonding displays slightly shorter wavelengths and higher absorption (E_{abs}) and emission (E_{em}) energies compared to C–O and C–C couplings. Interestingly, this trend is more pronounced in the smaller GQD-30 systems.

For absorption and emission spectra illustrated in Fig. 5, we can observe that addition of drug leads to a red shift of the absorption peaks compared to pure GQDs curve given in Fig. 2. Due to the fact that both the GQDs and DOX are

Table 3 Optical parameters of conjugated systems determined by TDDFT: the absorption energy E_{abs} and its corresponding wavelength λ_{abs}, the emission energy E_{em} and its corresponding wavelength λ_{em}, and the Stokes shift. Energies in eV and wavelength is nm

		E_{abs}	λ_{abs}	E_{em}	λ_{em}	Stokes shift
$C_{30}H_{14}$ + DOX	C–C	1.287	963.5	0.68	1808	0.685
	C–N	1.823	680	0.94	1311	0.878
	C–O	1.934	641	1.11	1120	0.828
$C_{48}H_{18}$ + DOX	C–C	1.092	1136	1.03	1199	0.059
	C–N	1.430	866	1.28	967	0.149
	C–O	1.429	867	1.27	971	0.153

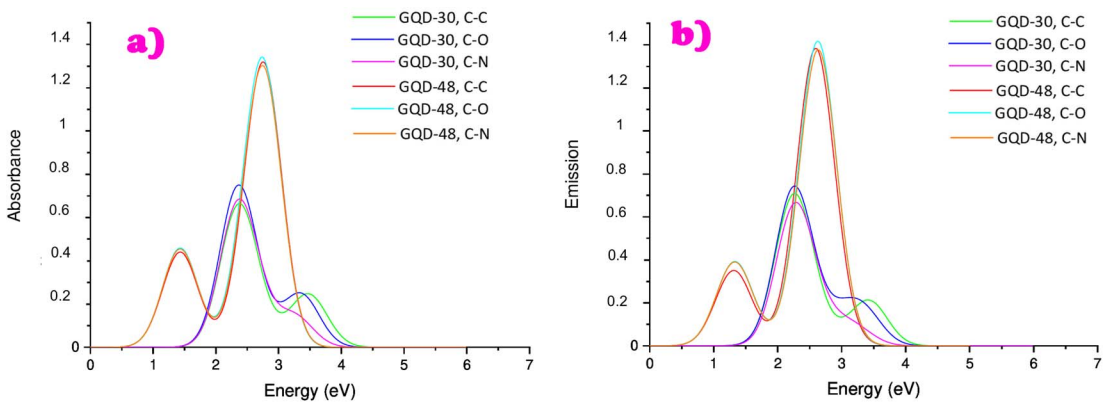

Fig. 5 Absorption and photoluminescence spectra of GQDs + DOX hybrids.

Open Access Article. Published on 28 April 2025. Downloaded on 1/19/2026 3:58:13 AM. This article is licensed under a Creative Commons Attribution-NonCommercial 3.0 Unported Licence.

photoluminescent, as shown by the emission energy of the pristine systems listed in Table 1, the emission wavelengths are greater than the wavelengths of absorption. Optical behaviour of GQDs + DOX hybrids covers a broad wavelength ranged from 400 nm to 1900 nm, demonstrating their adaptability. In addition, larger hybrids GQD-48 + DOX exhibit a greater optical gap compared to the smaller hybrids, which indicates the increased likelihood of electromagnetic absorption and emission between levels. This corresponds to more significant optical transitions as well as enhanced brightness in the bigger hybrids.

The observed decrease in absorption and emission energies for GQD-30 + DOX systems, particularly in configurations with C–C bonding, can be traced to the reduced HOMO–LUMO gap, which causes a redshift in optical transitions. This connection can be explained by the fundamental relationship between electronic and optical properties, where a smaller gap corresponds to lower excitation energies. The photoluminescence spectra further highlight the impact of quantum confinement, where smaller GQDs exhibit larger Stokes shifts. Precisely, the calculated Stokes shift between absorption and emission spectra presented in Table 3, is found to be larger in small-sized conjugations. This is suggestive of a rapid relaxation from the initial to the emissive state. Additionally, when the absorption and emission peaks are viewed more closely, it can be seen that the GQD-30 + DOX systems are characterized by one dominant intense peak within the [550, 558] nm range. The GQD-48 + DOX nanostructures, on the other hand, present two intense peaks at [464–466] nm and [890–900] nm. This aligns with experimental findings on GQDs.[49]

It is noteworthy that the type of coupling between GQDs and the drug, as well as the choice of QD size play a crucial role in tuning the optical properties. That is, hybridization significantly modifies the property of small-sized GQDs, with little change being observed for large-sized systems. This fact is helpful in designing the optoelectronic properties of GQDs for a target application.

4. Conclusion

In conclusion, this study analysed various structures of GQDs + DOX hybrid systems with two different sizes of DSGQDs, namely GQDs-30 and GQDs-48 to verify their optoelectronic and photoluminescence properties. We investigated the influence of the size of the GQDs relative to the loaded drug and the character of the interactions of covalent bonds C–C, C–O, and C–N couplings, on the physical behaviour of the hybrids. By incorporating these essential factors, six stable configurations were simulated with different electronic and optical properties. Notably, the H–L energy gap varied with DOX positioning, with smaller GQDs experiencing larger changes than their larger counterparts. The optical properties of the larger GQD systems remained largely intact with absorption and photoluminescence in the NIR region, whereas that of the smaller GQDs was shifted from the visible to the NIR region. These findings have significant implications for the selection of the best GQD functionalization strategies for use in nanomedical drug delivery systems.

Data availability

Data for this article, including results listed in the tables and the determined figures, are obtained using the Gaussian 09 software [**https://gaussian.com/g09citation/**] and Gaussview [**https://gaussian.com/citation/**]. The methods used in this study are density functional theory (DFT) and time-dependent density functional theory (TDDFT) at the the B3LYP exchange-correlation functional [**https://doi.org/10.1063/1.464304**] and 6-31G(d,p) as basis set [**https://doi.org/10.1063/1.1674902**].

Conflicts of interest

There are no conflicts to declare.

Acknowledgements

The authors would like to acknowledge the "Académie Hassan II des Sciences et Techniques", Morocco, for its financial support. The authors also thank the LPHE-MS, Faculty of Sciences, Mohammed V University in Rabat, Morocco, for technical support through their computer facilities, where all the calculations have been performed.

References

1 A. K. Geim and K. S. Novoselov, The rise of graphene, *Nat. Mater.*, 2007, **6**, 183–191.
2 P. K. Nayak, C. J. Hsu, S. C. Wang, J. C. Sung and J. L. Huang, Graphene coated Ni films: a protective coating, *Thin Solid Films*, 2013, **529**, 312–316.
3 K. S. Novoselov, D. Jiang, F. Schedin, T. J. Booth, V. V. Khotkevich, S. V. Morozov and A. K. Geim, Two-dimensional gas of massless Dirac fermions in graphene, *Nature*, 2005, **438**, 197–200.
4 T. Wang, D. Huang, Z. Yang, S. Xu, G. He, X. Li, N. Hu, G. Yin, D. He and L. Zhang, A review on graphene-based gas/vapor sensors with unique properties and potential applications, *Nano-Micro Lett.*, 2016, **8**, 95–119.
5 K. S. Novoselov, A. K. Geim, S. V. Morozov, D. Jiang, Y. Zhang, S. V. Dubonos, I. V. Grigorieva and A. A. Firsov, Electric field effect in atomically thin carbon films, *Science*, 2004, **306**, 666–669.
6 F. Xia, H. Wang, D. Xiao, M. Dubey and A. Ramasubramaniam, Two-dimensional material nanophotonics, *Nat. Photonics*, 2014, **8**, 899–907.
7 M. Kakran and L. Li, Carbon nanomaterials for drug delivery, *Key Eng. Mater.*, 2012, **508**, 76–80.
8 H. Shen, L. Zhang, M. Liu and Z. Zhang, Biomedical applications of graphene, *Theranostics*, 2012, **2**, 283.
9 Y.-M. Lin, C. Dimitrakopoulos, K. A. Jenkins, D. B. Farmer, H.-Y. Chiu, A. Grill and P. Avouris, 100 GHz Transistors from Wafer Scale Epitaxial Graphene, *Science*, 2010, **327**, 662.
10 Z. Zeng, S. Chen, T. T. Y. Tan and F.-X. Xiao, Graphene quantum dots (GQDs) and its derivatives for multifarious photocatalysis and photoelectrocatalysis, *Catal. Today*, 2018, 171.

© 2025 The Author(s). Published by the Royal Society of Chemistry

Open Access Article. Published on 28 April 2025. Downloaded on 1/19/2026 3:58:13 AM. This article is licensed under a Creative Commons Attribution-NonCommercial 3.0 Unported Licence.

11 J. Wang, R. Zhao, R. Yang, R. Liu and Z. Liu, Inverse relationship between carrier mobility and bandgap in graphene, *J. Chem. Phys.*, 2013, **138**, 084701.
12 R. R. Nair, P. Blake, A. N. Grigorenko, K. S. Novoselov, T. J. Booth, T. Stauber, N. M. Peres and A. K. Geim, Fine structure constant defines visual transparency of graphene, *Science*, 2008, **320**, 1308.
13 M. Shahrokhi and C. Leonard, Tuning the band gap and optical spectra of silicon-doped graphene: many-body effects and excitonic states, *J. Alloys Compd.*, 2017, **693**, 1185–1196.
14 C. K. Chua, Z. Sofer, P. Simek, O. Jankovsky, K. Klimova, S. Bakardjieva, S. H. Kuckova and M. Pumera, Recent advances in carbon-based dots for electroanalysis, *ACS Nano*, 2015, **9**, 2548.
15 M. Y. Han, B. Özyilmaz, Y. Zhang and P. Kim, Energy band-gap engineering of graphene nanoribbons, *Phys. Rev. Lett.*, 2007, **98**, 206805.
16 Y. Volkov, Quantum dots in nanomedicine: recent trends, advances and unresolved issues, *Biochem. Biophys. Res. Commun.*, 2015, **468**, 419–427.
17 M. Bacon, S. J. Bradley and T. Nann, Graphene Quantum Dots, *Part. Part. Syst. Charact.*, 2014, **31**, 415–428.
18 A. D. G. Potasz and P. Hawrylak, Excitonic absorption in gate-controlled graphene quantum dots, *Phys. Rev. B: Condens. Matter Mater. Phys.*, 2010, **82**, 155445.
19 C. Mansilla Wettstein, F. P. Bonaf, B. Oviedo and C. G. Sanchez, Optical properties of graphene nanoflakes: shape matters, *J. Chem. Phys.*, 2016, **144**, 224305.
20 T. Basak, H. Chakraborty and A. Shukla, Theory of linear optical absorption in diamond-shaped graphene quantum dots, *Phys. Rev. B: Condens. Matter Mater. Phys.*, 2015, **92**, 205404.
21 S. S. Yamijala, A. Bandyopadhyay and S. K. Pati, Structural stability, electronic, magnetic, and optical properties of rectangular graphene and boron nitride quantum dots: effects of size, substitution, and electric field, *J. Phys. Chem. C*, 2013, **117**, 23295–23304.
22 L. A. Ponomarenko, F. Schedin, M. I. Katsnelson, R. Yang, E. W. Hill, K. S. Novoselov and A. K. Geim, Chaotic Dirac billiard in graphene quantum dots, *Science*, 2008, **320**, 356–358.
23 F. Z. Ramadan, H. Ouarrad and L. B. Drissi, Tuning Optoelectronic Properties of the Graphene-Based Quantum Dots $C_{16x}Si_xH_{10}$ Family, *J. Phys. Chem. A*, 2018, **122**, 5016–5025.
24 H. Ouarrad, F. Z. Ramadan and L. B. Drissi, Engineering silicon-carbide quantum dots for third generation photovoltaic cells, *Opt. Express*, 2020, **28**, 36656–36667.
25 L. Li, J. Ji, R. Fei, C. Wang, Q. Lu and J. Zhang, A facile microwave avenue to electrochemiluminescent two-color graphene quantum dots, *Adv. Funct. Mater.*, 2012, **22**, 2971.
26 J. Shen, Y. Zhu, X. Yang and C. Li, Graphene quantum dots: emergent nanolights for bioimaging, sensors, catalysis and photovoltaic devices, *Chem. Commun.*, 2012, **48**, 3686.
27 J. Ryu, J. W. Lee, H. Yu, J. Yun, K. Lee, J. Lee, D. Hwang, J. Kang, S. K. Kim and J. Jang, Size effects of a graphene quantum dot modified-blocking TiO_2 layer for efficient planar perovskite solar cells, *J. Mater. Chem. A*, 2017, **5**, 16834–16842.
28 R. Hardman, A toxicologic review of quantum dots: toxicity depends on physicochemical and environmental factors, *Environ. Health Perspect.*, 2006, **114**, 165–172.
29 M. Zhang, L. Bai, W. Shang, W. Xie, H. Ma, Y. Fu, D. Fang, H. Sun, L. Fan, M. Han, C. Liu and S. Yang, Facile synthesis of water-soluble, highly fluorescent graphene quantum dots as a robust biological label for stem cells, *J. Mater. Chem.*, 2012, **22**, 7461–7467.
30 S. Nikazar, V. S. Sivasankarapillai, A. Rahdar, S. Gasmi, P. S. Anumol and M. S. Shanavas, Revisiting the cytotoxicity of quantum dots: an in-depth overview, *Biophys. Rev.*, 2020, **12**, 703.
31 H. Ouarrad, F. Z. Ramadan and L. B. Drissi, Size engineering optoelectronic features of C, Si and CSi hybrid diamond-shaped quantum dots, *RSC Adv.*, 2019, **9**, 28609–28617.
32 X. Yan, X. Cui and L. S. Li, Synthesis of large, stable colloidal graphene quantum dots with tunable size, *J. Am. Chem. Soc.*, 2010, **132**, 5944.
33 L. B. Drissi, H. Ouarrad, F. Z. Ramadan and W. Fritzsche, Graphene and silicene quantum dots for nanomedical diagnostics, *RSC Adv.*, 2020, **10**, 801–811.
34 B. Mandal, S. Sarkar and P. Sarkar, Exploring the electronic structure of graphene quantum dots, *J. Nanopart. Res.*, 2012, **14**, 1–8.
35 S. Kim, S. W. Hwang, M.-K. Kim, D. Y. Shin, D. H. Shin, C. O. Kim, S. B. Yang, *et al.*, Anomalous behaviors of visible luminescence from graphene quantum dots: interplay between size and shape, *ACS Nano*, 2012, **6**, 8203.
36 R. Zhang, S. Qi, J. Jia, B. Torre, H. Zeng, H. Wu and X. Xu, Size and refinement edge-shape effects of graphene quantum dots on UV-visible absorption, *J. Alloys Compd.*, 2015, **623**, 186.
37 H. Ouarrad, L. B. Drissi, R. Assad and W. Fritzsche, Photoluminescence mechanism and optoelectronic responses of Janus pyrene and Janus coronene QDs for OLEDs & nanomedical applications, *J. Phys. Chem. Solids*, 2024, **184**, 111675.
38 H. Safardoust-Hojaghan, M. Salavati-Niasari, O. Amiri and M. Hassanpour, Preparation of highly luminescent nitrogen doped graphene quantum dots and their application as a probe for detection of *Staphylococcus aureus* and *E. coli*, *J. Mol. Liq.*, 2017, **241**, 1114.
39 X. Hai, Q.-X. Mao, W.-J. Wang, X. Feng Wang, X.-W. Chen and J.-H. Wang, An acid-free microwave approach to prepare highly luminescent boron-doped graphene quantum dots for cell imaging, *J. Mater. Chem. B*, 2015, **3**, 9109.
40 P. Gong, J. Peiwei, K. Hou, Z. Yang, Z. Wang, Z. Liu, X. Han and S. Yang, Small but strong: the influence of fluorine atoms on formation and performance of graphene quantum dots using a gradient F-sacrifice strategy, *Carbon*, 2017, **112**, 63–71.

© 2025 The Author(s). Published by the Royal Society of Chemistry

Open Access Article. Published on 28 April 2025. Downloaded on 1/19/2026 3:58:13 AM. This article is licensed under a Creative Commons Attribution-NonCommercial 3.0 Unported Licence.

41 Y. Haddad, H. Ouarrad and L. B. Drissi, Insights into the optoelectronic behaviour of heteroatom doped diamond-shaped graphene quantum dots, *RSC Adv.*, 2024, **14**, 12639.
42 D. Iannazzo, A. Pistone, C. CelestI, C. Triolo, S. Patané, S. V. Giofré, R. Romeo, I. Ziccarelli, R. Mancuso, B. Gabriele and G. Visalli, A smart nanovector for cancer targeted drug delivery based on graphene quantum dots, *Nanomaterials*, 2019, **9**(2), 282.
43 J. Sun, Q. Xin, Y. Yang, H. Shah, H. Cao, Y. Qi, J. R. Gong and J. Li J, Nitrogen-doped graphene quantum dots coupled with photosensitizers for one-/two-photon activated photodynamic therapy based on a FRET mechanism, *Chem. Commun.*, 2018, **54**(7), 715–718.
44 Z. Wang, J. Xia, C. Zhou, B. Via, Y. Xia, F. Zhang, Y. Li, L. Xia and J. Tang, Synthesis of strongly green-photoluminescent graphene quantum dots for drug carrier, *Colloids Surf., B*, 2013, **112**, 192–196.
45 M. Ruzycka-Ayoush, P. Kowalik, A. Kowalczyk, P. Bujak, A. M. Nowicka, M. Wojewodzka, M. Kruszewski and I. P. Grudzinski, Quantum dots as targeted doxorubicin drug delivery nanosystems in human lung cancer cells, *Cancer Nanotechnol.*, 2021, **12**, 1–27.
46 C. Yan, X. Hu, P. Guan, T. Hou, P. Chen, D. Wan, X. Zhang, J. Wang and C. Wang, Highly biocompatible graphene quantum dots: green synthesis, toxicity comparison and fluorescence imaging, *J. Mater. Sci.*, 2020, **55**, 1198–1215.
47 S. Fasbender, L. Zimmermann, R. P. Cadeddu, M. Luysberg, B. Moll, C. Janiak and R. Haas, The low toxicity of graphene quantum dots is reflected by marginal gene expression changes of primary human hematopoietic stem cells, *Sci. Rep.*, 2019, **9**, 12028.
48 S. Javadian, K. Najafi, S. M. Sadrpoor, F. Ektefa, N. Dalir and M. Nikkhah, Graphene quantum dots based magnetic nanoparticles as a promising delivery system for controlled doxorubicin release, *J. Mol. Liq.*, 2021, **331**, 115746.
49 A. M. Sawy, A. Barhoum, S. A. Gaber, S. M. El-Hallouty, W. G. Shousha, A. A. Maarouf and A. S. Khalil, Insights of doxorubicin loaded graphene quantum dots: synthesis, DFT drug interactions, and cytotoxicity, *Mater. Sci. Eng., C*, 2021, **122**, 111921.
50 F. Khodadadei, S. Safarian and N. Ghanbari, Methotrexate-loaded nitrogen-doped graphene quantum dots nanocarriers as an efficient anticancer drug delivery system, *Mater. Sci. Eng., C*, 2017, **79**, 280–285.
51 C. Wang, Y. Chen, Z. Xu, B. Chen, Y. Zhang, X. Yi and J. Li J, Fabrication and characterization of novel cRGD modified graphene quantum dots for chemo-photothermal combination therapy, *Sens. Actuators, B*, 2020, **309**, 127732.
52 R. Rakhshaei, H. Namazi, H. Hamishehkar and M. Rahimi, Graphene quantum dot cross-linked carboxymethyl cellulose nanocomposite hydrogel for pH-sensitive oral anticancer drug delivery with potential bioimaging properties, *Int. J. Biol. Macromol.*, 2020, **150**, 1121.
53 L. Qi and X. Gao, Emerging application of quantum dots for drug delivery and therapy, *Expert Opin. Drug Delivery*, 2008, **5**(3), 263.
54 P. Shivakumar, M. Usha Rani, A. Gopala Reddy and Y. Anjaneyulu, A Study on the Toxic Effects of Doxorubicin on the Histology of Certain Organs, *Toxicol. Int.*, 2012, **19**(3), 241.
55 A. M. Sawy, A. Barhoum, S. A. A. Gaber, S. M. El-Hallouty, W. G. Shousha, A. A. Maarouf and A. S. Khalil, Insights of doxorubicin loaded graphene quantum dots: synthesis, dft drug interactions, and cytotoxicity, *Mater. Sci. Eng., C*, 2021, **122**, 111921.
56 A. D. Becke, A new mixing of Hartree-Fock and local density-functional theories, *J. Chem. Phys.*, 1993, **98**, 1372.
57 C. Lee, W. Yang and R. G. Parr, Development of the Colle-Salvetti correlation-energy formula into a functional of the electron density, *Phys. Rev. B*, 1988, **37**, 785.
58 I. Y. Zhang, J. Wu and X. Xu, Extending the reliability and applicability of B3LYP, *Chem. Commun.*, 2010, **46**(18), 3057–3070.
59 Y. Zhang, X. Xu and W. A. Goddard III, Doubly hybrid density functional for accurate descriptions of nonbond interactions, thermochemistry, and thermochemical kinetics, *Proc. Natl. Acad. Sci. U. S. A.*, 2009, **106**(13), 4963–4968.
60 A. Dreuw and M. Head-Gordon, Single-reference *ab initio* methods for the calculation of excited states of large molecules, *Chem. Rev.*, 2005, **105**, 4009–4037.
61 M. Zhao, F. Yang, Y. Xue, D. Xiao and Y. Guo, A time-dependent dft study of the absorption and fluorescence properties of graphene quantum dots, *ChemPhysChem*, 2014, **15**, 950–957.
62 S. A. Aal, DFT study of the therapeutic potential of borospherene and metalloborospherenes as a new drug-delivery system for the 5-fluorouracil anticancer drug, *J. Mol. Liq.*, 2022, **360**, 119457.
63 S. H. Vosko, L. Wilk and M. Nusair, Accurate spin-dependent electron liquid correlation energies for local spin density calculations: a critical analysis, *Can. J. Phys.*, 1980, **58**, 1200–1211.
64 A. D. Becke, Density-functional thermochemistry I. The effect of the exchange-only gradient correction, *J. Chem. Phys.*, 1992, **96**, 2155–2160.
65 R. G. Parr, R. A. Donnelly, M. Levy and W. E. Palke, Electronegativity: the density functional viewpoint, *J. Chem. Phys.*, 1978, **68**, 3801–3807.
66 Y. Chong, Y. Ma, H. Shen, X. Tu, X. Zhou, J. Xu and Z. Zhang, The *in vitro* and *in vivo* toxicity of graphene quantum dots, *Biomaterials*, 2014, **35**, 5041–5048.
67 S. Baskoutas and A. F. Terzis, Size-dependent band gap of colloidal quantum dots, *J. Appl. Phys.*, 2006, **99**, 013708.
68 J. K. Bhattarai, D. Neupane, B. Nepal, A. V. Demchenko and K. J. Stine, Nanoporous Gold Monolith for High Loading of Unmodified Doxorubicin and Sustained Co-Release of Doxorubicin-Rapamycin, *Nanomaterials*, 2021, **11**(1), 208.
69 T. Sikora, K. Morawska, W. Lisowski, P. Rytel and A. Dylong, Application of Optical Methods for Determination of Concentration of Doxorubicin in Blood and Plasma, *Pharmaceuticals*, 2022, **15**, 112.

© 2025 The Author(s). Published by the Royal Society of Chemistry

Open Access Article. Published on 28 April 2025. Downloaded on 1/19/2026 3:58:13 AM. This article is licensed under a Creative Commons Attribution-NonCommercial 3.0 Unported Licence.

70 S. Shah, A. Chandra, A. Kaur, N. Sabnis, A. Lacko, Z. Gryczynski and I. Gryczynski, Fluorescence properties of doxorubicin in PBS buffer and PVA films, *J. Photochem. Photobiol., B*, 2017, **170**, 65–69.

71 S. H. Song, M. Jang, H. Yoon, Y.-H. Cho, S. Jeon and B.-H. Kim, Size and pH dependent photoluminescence of graphene quantum dots with low oxygen content, *RSC Adv.*, 2016, **6**, 97990–97994.

72 X. Wu X, F. Tian, W. Wang, J. Chen, M. Wu and J. X. Zhao, Fabrication of highly fluorescent graphene quantum dots using L-glutamic acid for *in vitro*/*in vivo* imaging and sensing, *J. Mater. Chem. C*, 2013, **1**(31), 4676–4684.

73 A. D. Gülcü, P. Potasz and P. Hawrylak, Excitonic absorption in gate-controlled graphene quantum dots, *Phys. Rev. B: Condens. Matter Mater. Phys.*, 2010, **82**, 155445.

74 S. Kim, S. W. Hwang, M.-K. Kim, D. Y. Shin, D. H. Shin, C. O. Kim, S. B. Yang, J. H. Park, E. Hwang, S. H. Choi and G. Ko, Anomalous behaviors of visible luminescence from graphene quantum dots: interplay between size and shape, *ACS Nano*, 2012, **6**(9), 8203.

75 J. D. Bargh, A. Isido-Llobet, J. S. Parker and D. R. Spring, Cleavable linkers in antibody–drug conjugates, *Chem. Soc. Rev.*, 2019, **48**(16), 4361–4374.

76 Z. Wang, C. Zhou, J. Xia, B. Via, Y. Xia, F. Zhang, Y. Li and L. Xia, Fabrication and characterization of a triple functionalization of graphene oxide with Fe_3O_4, folic acid and doxorubicin as dual-targeted drug nanocarrier, *Colloids Surf., B*, 2013, **106**, 60–65.

77 F. Gao, C. L. Yang and G. Jiang, Effects of the coupling between electrode and GQD-anthoxanthin nanocomposites for dye-sensitized solar cell: DFT and TD-DFT investigations, *J. Photochem. Photobiol., A*, 2021, **407**, 113080.

78 F. Gao, C. L. Yang, M. S. Wang, X. G. Ma and W. W. Liu, Theoretical studies on the feasibility of the hybrid nanocomposites of graphene quantum dot and phenoxazine-based dyes as an efficient sensitizer for dye-sensitized solar cells, *Spectrochim. Acta, Part A*, 2019, **206**, 216–223.

79 M. Vatanparast and Z. Shariatinia, Hexagonal boron nitride nanosheet as novel drug delivery system for anticancer drugs: insights from DFT calculations and molecular dynamics simulations, *J. Mol. Graphics Modell.*, 2019, **89**, 50–59.

80 S. Karimzadeh, B. Safaei and T. C. Jen, Theorical investigation of adsorption mechanism of doxorubicin anticancer drug on the pristine and functionalized single-walled carbon nanotube surface as a drug delivery vehicle: a DFT study, *J. Mol. Liq.*, 2021, **322**, 114890.

81 A. S. Abdel-Bary, D. A. Tolan, M. Y. Nassar, T. Taketsugu and A. M. El-Nahas, Chitosan, magnetite, silicon dioxide, and graphene oxide nanocomposites: synthesis, characterization, efficiency as cisplatin drug delivery, and DFT calculations, *Int. J. Biol. Macromol.*, 2020, **154**, 621–633.

82 K. G. Kim, X. Ma, C. Chen, Y. Ie, E. W. Coir, H. Hashemi, Y. Aso, P. F. Green, J. Kieffer and J. Kim, Energy Level Modulation of HOMO, LUMO, and Band-Gap in Conjugated Polymers for Organic Photovoltaic Applications, *Adv. Funct. Mater.*, 2013, **23**(4), 439–445.

83 M. Lotfia, A. Morsalia and M. R. Bozorgmehr, Comprehensive quantum chemical insight into the mechanistic understanding of the surface functionalization of carbon nanotube as a nanocarrier with cladribine anticancer drug, *Appl. Surf. Sci.*, 2018, **462**, 720–729.

84 D. Pegu, J. Deb, C. Van Alsenoy and U. Sarkar, Theoretical Investigation of Electronic, Vibrational and Nonlinear Optical Properties of 4-Fluoro-4-hydroxybenzophenone, *Spectrosc. Lett.*, 2017, **50**, 232–243.

85 V. Choudhary, A. Bhatt, D. Dash and N. Sharma, DFT calculations on molecular structures, HOMO–LUMO study, reactivity descriptors and spectral analyses of newly synthesized diorganotin(IV) 2-chloridophenylacetohydroxamate complexes, *J. Comput. Chem.*, 2019, **40**, 2354–2363.